Numerical Simulation of Ionized Rocket Plumes

D Gueyffier, B Fromentin-Denoziere, J Simon, A. Merlen, V Giovangigli

Numerical Simulation of Ionized Rocket Plumes

D. Gueyffier,* B. Fromentin-Denoziere,† J. Simon,† and A. Merlen‡
ONERA–The French Aerospace Lab, 91128 Palaiseau Cedex, France
and
V. Giovangigli§
École Polytechnique, 91128 Palaiseau, France

DOI: 10.2514/1.T4239

In this paper, a multiphysics numerical approach for predicting the ionization level in solid rocket engine plumes is presented. Ionization takes place in the rocket combustion chamber and in the exhaust plume. A low-temperature, high-density plasma is created, with small Debye length in most of the plume region. Ambipolar diffusion is therefore assumed for ions and electrons in the plume, and a set of conservation equations is derived to be solved by the numerical model. A number of numerical strategies to resolve this system is derived, as well as a novel scheme that enforces charge neutrality. This approach is integrated into a complex code for compressible, multispecies, turbulent flow simulations. The model is then coupled with a Maxwell's equations solver in order to simulate the radar cross section of rocket plumes. Finally, computations of ionization levels and radar cross section of a Black Brant rocket plume are presented.

I. Introduction

THERMAL ionization occurs in solid rocket chambers and exhaust plumes because of the low ionization energy of some chemical compounds present in solid propellant. Among them are alkali metals like sodium (Na) and potassium (K), which can be found in small amounts in propellant. Na and K easily lose one electron to form Na+ and K+ ions in the chamber and in the plume. A secondary combustion called afterburning occurs in the plume when combustion exhaust mix with outside oxygen, creating temperature elevations in regions and increasing production of electrons.

Because of their interest for various applications, among which is the computation of radar cross sections (RCSs) of rockets, these ionized plumes have been studied in previous work spanning four decades [1–6]. A careful review of the nonequilibrium chemical mechanisms describing ionization in the plume can be found in [7]. More recent work on numerical simulation can be found in [8–10]. Other closely related work includes [11–13]. Nevertheless, none of these works have provided a careful description of the plasma model and of the conservation equations relevant to the problem. Moreover, previous works did not examine whether fundamental properties of the ionized flow, like charge neutrality, were verified in their computations. In this paper, we demonstrate that the mixture forms a high-density, low-temperature plasma with small Debye length in the bulk of the plume. The relevant governing equations are the ones for multispecies flows under ambipolar diffusion conditions [14], as will be shown in the paper.

In addition, this paper presents a numerical scheme that resolves the governing equations for the ionized gas mixture. This scheme is then used to simulate the ionized plume of a Black Brant rocket at two altitudes (7.9 and 25.5 km) for two concentrations (100 and 10 ppm) of alkali metals in the propellant. Then, coupling the approach with a Maxwell's equations solver allows for the computation of the plume RCS.

The contributions of this paper are 1) a plasma model relevant to the flow in the rocket plume, 2) a numerical methodology to ensure charge neutrality in the flow, and 3) a time implicit integration scheme using an exact Jacobian, taking into account the charge neutrality constraint.

The paper is organized as follows:

Section II describes the ambipolar plasma model and the conservation equations. Section III details the chemical mechanism involving charged species in the plume. Section IV presents the numerical model and the strategy used to enforce zero charge and zero current constraints in our time implicit scheme. Validations of the numerical model are presented in Sec. V, including comparison with prior work on ionized rocket plumes. Computations of a rocket plume electron concentration field and radar signature are presented in the last section.

II. Ionization Model

A. Equilibrium Composition in the Chamber

Electrons and ions are formed due to high temperatures in the rocket combustion chamber. These charged species result from the thermal ionization of small amounts of alkali metals contained as impurities in the solid propellant. Computation of equilibrium concentrations in the chamber, including ions and electrons, is performed by minimizing Gibbs free energy. To obtain these concentrations, we use the chemical equilibrium code EQUIL contained in the CHEMKIN II package. EQUIL minimizes Gibbs free energy using constrained minimization. It makes use of the propellant chemical composition, formation enthalpies of species, and other thermodynamic data.

B. Ambipolar Diffusion in the Plume

In the nozzle and in the plume, we assume that the ionized mixture forms a low-temperature, high-density plasma, so that the Debye length is small. These assumptions have been verified a posteriori and our numerical simulations have shown that the Debye length is about 10^{-5} m in the bulk of the plume. Therefore, the plasma mixture must be quasi neutral and the current must be zero. An ambipolar electric polarization field must exist in the mixture to enforce zero current.

The diffusion current $\boldsymbol{j}$ is a linear combination of the species diffusion velocities and can be written in compact form as $\boldsymbol{j} = \langle \boldsymbol{z}, \boldsymbol{V} \rangle$ where $\boldsymbol{z} = (\rho_1 z_1, \ldots, \rho_n z_n)$ is the charge vector whose components $\rho_i z_i$ are the elementary charge per unit volume of each species, $\boldsymbol{V} = (\boldsymbol{V}_1, \ldots, \boldsymbol{V}_n)$ is the vector of species diffusion velocities, n is

Presented as Paper 2013-3129 at the 44th AIAA Plasmadynamics and Lasers Conference, San Diego, CA, 24–27 June 2013; received 24 July 2013; revision received 25 November 2013; accepted for publication 26 November 2013; published online 15 January 2014.

*Scientist, Rocket Propulsion Unit.
†Scientist, Department of Electromagnetics.
‡Professor and Chief Scientist, Fluid Mechanics Branch.
§Professor, Department of Applied Mathematics, Centre de Mathematiques Appliquees.

the total number of species in the mixture, and $< ., . >$ is the Euclidian scalar product.

Following [9], we write the diffusion velocity vector in the form

$$\boldsymbol{V} = -\boldsymbol{D}\left(\boldsymbol{d} - z\frac{\boldsymbol{E}}{p}\right) \tag{1}$$

where $\boldsymbol{D}$ is the multicomponent diffusion matrix and $\boldsymbol{d} = (\nabla p_1/p, \ldots, \nabla p_n/p)$ is the vector of partial pressure gradients normalized by the pressure. We deduce an expression for the ambipolar electric field from the zero current condition

$$\boldsymbol{j} = \boldsymbol{0} \Rightarrow \boldsymbol{E} = p\frac{\langle \boldsymbol{z}, \boldsymbol{D}\boldsymbol{d}\rangle}{\langle \boldsymbol{z}, \boldsymbol{D}\boldsymbol{z}\rangle} \tag{2}$$

As seen in expression (2), the ambipolar field has a purely diffusive contribution. Introducing the auxiliary matrix $\breve{\boldsymbol{D}} = \boldsymbol{D} - (\boldsymbol{D}\boldsymbol{z} \otimes \boldsymbol{D}\boldsymbol{z})/\langle \boldsymbol{z}, \boldsymbol{D}\boldsymbol{z}\rangle$, the diffusion velocity now reads

$$\boldsymbol{V} = -\breve{\boldsymbol{D}}\boldsymbol{d} \tag{3}$$

so that the system of conservation equations (mass, momentum, and energy) can be written as

$$\begin{cases} \partial_t(\rho y_i) + \nabla.(\rho y_i \boldsymbol{v}) + \nabla.(\rho y_i \boldsymbol{V_i}) = m_i\omega_i, & i = 1, \ldots, n \\ \partial_t(\rho \boldsymbol{v}) + \nabla.(\rho \boldsymbol{v} \otimes \boldsymbol{v} + p\boldsymbol{I}) + \nabla.\Pi = \boldsymbol{0}, \\ \partial_t\left(\frac{1}{2}\rho \boldsymbol{v}.\boldsymbol{v} + E\right) + \nabla.\left(\left(\frac{1}{2}\rho \boldsymbol{v}.\boldsymbol{v} + E + p\right)\boldsymbol{v}\right) + \nabla.(\boldsymbol{q} + \Pi.\boldsymbol{v}) = 0 \end{cases} \tag{4}$$

where y_i is the mass fraction of the ith species, $\rho_i = \rho y_i$ is its mass density, $\rho = \sum \rho_i$ is the mass density of the mixture, m_i is the molar mass of the ith species, Π is the viscous tensor, and E is the internal energy per unit volume. We observe in this set of equations that no Gauss–Poisson equation is necessary to calculate the electric field because the $\boldsymbol{E}$ field is hidden inside the diffusion velocity $\boldsymbol{V}$. In addition, multiplying by the mass conservation equation z_i for the ith species and summing on all $i = 1...n$, we form the conservation equation for total charge per unit volume $q = \sum \rho_i z_i$, which takes the form $\partial_t q + \nabla.(q\boldsymbol{v}) = 0$. With zero charge q on all domain boundaries, we obtain that $q = 0$. Total charge is zero everywhere. We can also remove the mass equations for one charged species from the system and replace it with equation $q = 0$, which is the strategy we will adopt in Sec. IV.

C. Turbulent Filtering

In the plume, turbulence ensures the mixture of reactive gases with the ambient fluid. For this type of flow, direct numerical simulation is beyond the scope. Instead, we adopt the classical RANS approach to model turbulence. To derive the equations for the RANS model, we apply turbulent filtering to the fundamental equations (4) for the ambipolar mixture.

We denote by $\tilde{\phi}$ the Reynolds (time) average of any quantity ϕ, by $\tilde{\phi} = \overline{\rho\phi}/\bar{\rho}$ its Favre average, its Reynolds fluctuations by $\phi' = \phi - \bar{\phi}$, and its Favre fluctuations by $\phi'' = \phi - \tilde{\phi}$. Applying the Reynolds averaging operator to the ith species mass conservation equation, we obtain

$$\partial_t(\bar{\rho}\tilde{y}_i) + \nabla.(\bar{\rho}\tilde{y}_i\tilde{\boldsymbol{v}}) + \nabla.(\overline{\rho y_i'' \boldsymbol{v}''}) + \overline{\nabla.(\rho y_i \boldsymbol{V_i})} = m_i\bar{\omega}_i \tag{5}$$

Ionization chemistry is considered slow and therefore we assume

$$\bar{\omega}_i(\rho, y_1, \ldots, y_n, T) = \omega_i(\bar{\rho}, \bar{y}_1, \ldots, \bar{y}_n, \bar{T}) \tag{6}$$

The Reynolds flux of y_i is modeled by analogy with Fick's law using the classical Boussinesq approximation

$$\overline{\rho y_i'' \boldsymbol{v}''} = -\frac{\mu_t}{Sc_t}\nabla\tilde{y}_i \tag{7}$$

with μ_t as the turbulent viscosity, which needs to be modeled and Sc_t as the turbulent Schmidt number.

For momentum and energy, we use the Reynolds averaged equations described in [15].

D. Neglecting Molecular Diffusion

For large Reynolds numbers, molecular diffusion is negligible so that the $\overline{\nabla.(\rho y_i \boldsymbol{V_i})}$ term in Eq. (5) is very small compared to other terms. However, even with negligible molecular diffusion, turbulent filtering by the turbulence model conserves charge, as well as the zero current constraint. This can be shown by multiplying the mass conservation equation for the ith species (4) by z_i and taking the Favre average of the resulting equation.

Hence, the main conclusion of this section is that even if molecular diffusion is small compared to turbulent diffusion, the set of filtered equations has the property of ensuring charge neutrality and zero current.

III. Ionization Chemistry

We present briefly the set of chemical reactions used to describe ionization of alkali metal and in the nozzle region and plume. These reactions were obtained from previous work on ionization of alkali metals in rocket plumes [2,7,16,17]. The mechanism involves the following reactions

$$\mathrm{K_+ + e_- + M \leftrightarrow K + M\,[7]} \quad \mathrm{K_+ + Cl_- \leftrightarrow K + Cl\,[7]}$$

$$\mathrm{K_+ + Cl_- + M \leftrightarrow KCl + M\,[7]} \quad \mathrm{Cl + e_- + M \leftrightarrow Cl_- + M\,[7]}$$

$$\mathrm{HCl + e_- \leftrightarrow Cl_- + H\,[7]} \quad \mathrm{K + HCl \leftrightarrow KCl + H\,[16]}$$

$$\mathrm{Na_+ + e_- + M \leftrightarrow Na + M\,[7]} \quad \mathrm{Na_+ + Cl_- \leftrightarrow Na + Cl\,[7]}$$

$$\mathrm{Na_+ + Cl_- + M \leftrightarrow NaCl + M\,[7]}$$

$$\mathrm{Na + HCl \leftrightarrow NaCl + H\,[17]} \quad \mathrm{Na + Cl + M \leftrightarrow NaCl + M\,[7]}$$

$$\mathrm{Na_+ + K \leftrightarrow Na + K_+\,[2]}$$

These reactions supplement another set of chemical reactions used to simulate afterburning. This mechanism contains 17 reactions and involves 12 species (N_2, H_2, O_2, O, H_2O, OH, H, CO, CO_2, HCl, Cl_2, Cl). An Arrhenius–Kooij law is used to describe the temperature dependence of chemical reaction rates

$$K_r(T) = A_r T^{\beta_r} \exp\left(-\frac{E_{A,r}}{RT}\right) \tag{8}$$

with K_r as the rate constant of the rth reaction, A_r as the pre-exponential factor, β_r as the temperature exponent, and $E_{A,r}$ as the activation energy. The set of chemical reactions is formally written as

$$\sum_{i\in S} \nu_{ij}^f \Omega_j \Leftrightarrow \sum_{i\in S} \nu_{ij}^b \Omega_j, \qquad j \in R \tag{9}$$

with $S = \{1, .., n\}$ as the set of species indices, ν_{ij}^f and ν_{ij}^b as the forward and backward stoichiometric coefficients of the ith species in the jth reaction, and $R = \{1, .., n^r\}$ as the set of chemical reactions indices. Then, the stoichiometric coefficients are denoted by

$$\nu_{ij} = \nu_{ij}^f - \nu_{ij}^b \tag{10}$$

The coherence of thermodynamic parameters has been thoroughly checked and compared to [18,19]. The reverse reaction rate constants have been evaluated using the equilibrium constant obtained from thermodynamics. We have also performed validation tests described in Sec. V.

IV. Numerical Model and Charge Neutrality

A. Numerical Model

The resolution of the conservation equations described previously is carried out using CEDRE, a numerical tool designed to simulate supersonic reactive gas flows [20,21]. This tool has been used to simulate a number of problems involving liquid and solid propulsion systems [22,23]. The solver performs calculations on unstructured meshes with cells of arbitrary geometry — in the present case, a triangular mesh with maximum refinement within the nozzle and in the plume region. The geometry is two-dimensional (2-D) axisymmetric with respect to the axis of the rocket. We have chosen a Harten–Lax–van Leer Contact (HLLC) [24] nonlinear Riemann solver that has proven very robust for the treatment of shocks and rarefaction waves. We also make use of a van Leer slope limiter to prevent spurious oscillations due to shocks. Time integration is first-order implicit (Backward Euler) and the nonlinear system of equations is solved using a Newton–Krylov method. In fact, the system is linearized using Newton's method and the resulting Jacobian is inverted using GMRES. In addition, this solver tracks alumina particles using an Eulerian approach [25], with coupled interactions between particle dynamics and fluid flow, including particle coalescence and atomization and particle interactions with liquid films [26,27].

Turbulence creation and transport is evaluated using a k-ε model that makes use of corrected coefficients to account for the 2-D axisymmetric geometry [28]. This model has proven reliable and accurate for a number of rocket flows simulations.

B. Computational Mesh

We make use of an unstructured mesh built using GMSH [29]. The mesh contains about 200,000 triangles. The mesh has been built to be more refined in the nozzle area and in the mixing layer close to the nozzle exit (see Fig. 1). The mesh becomes coarser with increasing distance to the nozzle, both along the axis and in the radial direction (see Fig. 2).

Domain decomposition is used to perform parallel computations. A total of 128 domains are used and the computation is performed on 128 Westmere cores of the ONERA Stelvio cluster. Restitution time is about 200 h and total CPU time is about 25,600 h. Although the mesh is relatively coarse, restitution time is quite long. In fact, we need to solve conservation equations for 21 chemical species, making the computation between 15 to 20 times longer than for a single gas.

C. Charge Neutrality

As previously shown, the system of conservation equations conserves charge. In addition, we show in this paragraph that the chemical production rates conserve charge by construction.

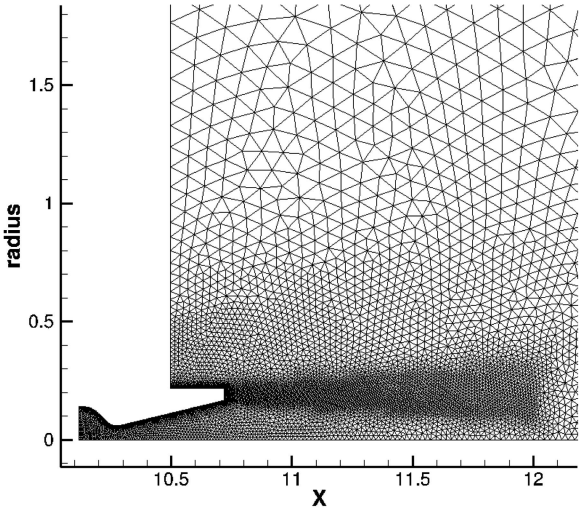

Fig. 1 Zoom on the mesh in the nozzle region, showing that the mesh is refined near nozzle walls and in the mixing layer.

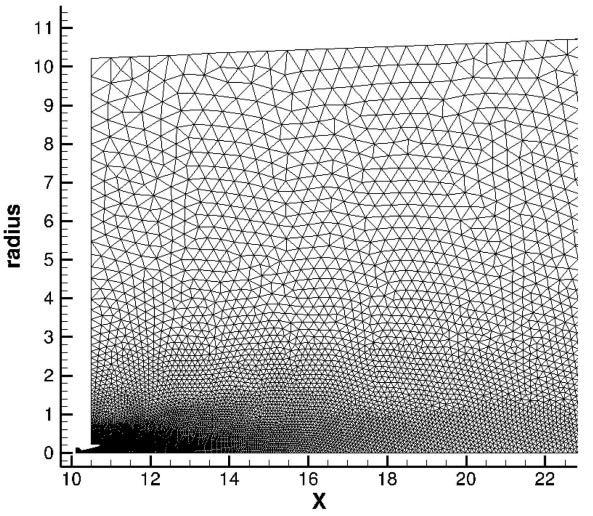

Fig. 2 Zoom on the mesh near the nozzle exit.

We denote by a_{il} the number of atom l in species i, the charge being treated as an atom, and by ν_r the vector of stoichiometric coefficients for the rth reaction defined by expression (10). Then conservation of atoms in the r reaction is expressed by the relation

$$\langle \boldsymbol{a}_l, \nu_r \rangle = 0 \tag{11}$$

The chemical rate of production of the ith species, denoted by ω_i, is a linear combination of the stoichiometric coefficients. In fact, the vector of production rates can be written as

$$\omega = \sum_r \tau_r \nu_r \tag{12}$$

with τ_r as the production rate of reaction r.

Using Eqs. (11) and (12) and the linearity of the scalar product operator, we obtain

$$\langle \boldsymbol{a}_l, \boldsymbol{\omega} \rangle = 0 \tag{13}$$

If we choose index l to be the one corresponding to the charge of each species, i.e., $\boldsymbol{a}_l = \boldsymbol{z}$, it follows that charge is conserved by the set of chemical reactions.

Hence, by mathematical construction, our solver should be conserving charge exactly. However, we show in the next paragraph that slope limiters used by compressible flow solvers tend to break charge neutrality in the plume.

D. Preliminary Simulations of Plume

We perform preliminary simulations in order to verify charge neutrality throughout the plume. Here, we resolve the conservation equations for all n species.

Figure 3 shows three cross sections along a rocket plume computed with our numerical approach at several distances from the nozzle exit. In this figure, we compare anions (including electrons) with cations concentrations in each cross section. The anions curve is expected to match exactly the cations curve. However, we observe some discrepancy in regions of large density gradients, mostly around the edge of the plume.

This small discrepancy indicates that charge is not properly conserved at the edge of the plume. Although the system of equations satisfies charge conservation, the numerical scheme introduces nonconservation of charged species. This type of phenomenon is often observed in regions of large density gradients with flux schemes using slope limiters [30]. In the following paragraph, we present a novel strategy to resolve this problem, by numerically enforcing the charge constraint.

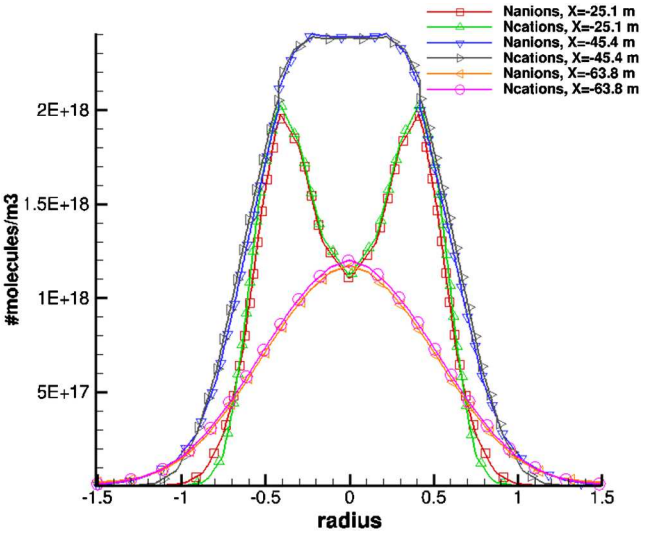

Fig. 3 Anion (including electrons) vs cation concentrations (in #molecules/m3) in cross sections along the plume.

E. Neutrality Constraint

As shown in Sec. II, a mass conservation equation for one species can be removed from the system and replaced by equation $q = 0$. To prevent nonconservation due to slope limiters, we choose to stop transporting electron mass. In fact, small electron mass may lead to computations of quantities that are comparable to machine epsilon and risk being rounded off. Electron concentration at each space location is deduced from the concentration of ions through the $q = 0$ constraint.

To compute the electron concentration, we write the charge constraint as

$$q = \sum_i z_i \rho_i = 0 \tag{14}$$

Equation (14) can be written under the form

$$q = \sum_i \alpha_i e N_A c_i = 0 \tag{15}$$

with $\alpha_i = \pm 1$ as the charge number (valence) of the ith species, e as the electron elementary charge, N_A as the Avogadro number, and c_i as the molar concentration of the ith species. In the present case, the charged species are $e-$, Cl−, Na+, and K+ so that the concentration of electrons can be deduced from (15), yielding

$$c_{e-} = c_{\mathrm{Na}+} + c_{\mathrm{K}+} - c_{\mathrm{Cl}-} = \sum_{\text{ions}} \alpha_i c_i \tag{16}$$

Electrons react with other species through the set of chemical equations presented in Sec. III. Electron concentration must be replaced by expression (16) in the computation of the production rate, as shown next. Decomposing the vector of molar concentrations as $\boldsymbol{c} = (c_h, c_{e-})$ and the production rate as $\boldsymbol{\omega} = (\omega_h, \omega_{e-})$, where h is the set of indices for the heavy species, we replace the electron concentration by expression (16) in the production rate

$$\omega_h^* = \omega_h\left(c_h, \sum_{\text{ions}} \alpha_i c_i\right) \tag{17}$$

F. Time-Implicit Scheme

To allow for large enough time steps, we make use of an implicit time marching scheme and linearize the nonlinear system of conservation equations using Newton's method. To do so, we have to form the Jacobian of the production rate with respect to concentrations $\boldsymbol{J} = \partial_c \boldsymbol{\omega}$. Electron concentration must be replaced in the computation of the Jacobian by the concentrations of the ions through expression (16) and, using the chain rule, we obtain

$$\partial_{ch}\boldsymbol{\omega}_h^* = \partial_{ch}\boldsymbol{\omega}_h + \partial_{ce-}\boldsymbol{\omega}_h \otimes \boldsymbol{\alpha} \tag{18}$$

whose elements are $(\partial_{ch}\boldsymbol{\omega}_h^*)_{ij} = \partial_{chj}\boldsymbol{\omega}_{hi} + \partial_{ce-}\boldsymbol{\omega}_{hi}\alpha_j$

Using expressions (16) and (18) in our numerical scheme enforces exact charge conservation. Electron concentration is deduced from heavy ions concentrations and electrons react with other species through the ionization chemistry. In addition, using expression (18) leads to good convergence of the Newton–Krylov method for the time implicit scheme, whereas failing to use the exact Jacobian expression (18) leads to divergence and failure of the computations. Validations of this scheme are presented in the next section.

V. Validation

A. Validation of Chemical Mechanism

We have verified that the ionization chemistry has been correctly integrated in our solver using the following test case, which in addition proves that we have used correct thermodynamic properties for the new charged species, alkali metals, and salts. We compare simulations obtained with our code (CEDRE code) of a homogeneous chemical reactor with a simulation performed using the CHEMKIN II package (SENKIN code). Initial conditions for both codes correspond to the chemical equilibrium in the combustion chamber of a Black Brant rocket. We change the temperature and pressure to the conditions at the throat, and we let the two methods relax to a new chemical equilibrium. We obtain very close results for the electron mass fraction using CEDRE and SENKIN at all times during the transient leading to the new equilibrium (see Fig. 4). The relative error between the results obtained using the two codes is of the order 2.10^{-2}.

B. Testing Charge Neutrality Constraint

We perform a new test similar to the preliminary test described in Sec. IV. Now we make use of the $q = 0$ charge constraint, and we enforce relations (16) and (18) in our scheme. We measure again the concentration of charged species in a cross section of a rocket plume. In this test, we want to verify that 1) charge discrepancies have disappeared and 2) charged species concentrations are of the same order of magnitude as without the constraint. Comparison of cation vs anion (including electron) concentration is shown in Fig. 5. Note that in this calculation, the influence of alumina particles is not taken into account.

Figure 5 shows that the concentrations of anions (including electrons) and cations are equal when enforcing the constraint. It also shows that the distribution of charged particles in the cross section is very similar with or without constraint. However, when the constraint is enforced, the concentration of charged particles is smaller along the plume centerline.

C. Comparison with Prior Work

We compare electron density (curve with circle symbols in Fig. 6) obtained with our approach for a Black Brant rocket plume at altitude 24.2 km with the results of [3].

Data for the Black Brant rocket in this test case and for all results shown in Sec. V originate from several publications. We chose data from [31] for the total mass of propellant $m_p = 997$ kg. The total duration of the combustion phase ($t = 32.4$ s) can be found in [32,33]. Data from [34] helped us calculate the mass flow rate $\dot{m} = 33,62$ kg/s and the rocket specific impulse Isp $= 271.3$ s (for a frozen expansion) and 277.3 s (for an equilibrium expansion) at altitude 24 km.

For the chamber pressure, we use $p_c = 44.82$ bar. The nozzle geometry is deduced from data in [33,35]. The nozzle length is 23.3 in., the diameter at the nozzle entrance is 11 in., the area ratio of the exit to the throat is 7.8, and the angle of the divergent section with respect to the axis is 13.5 deg. We obtained the chemical composition

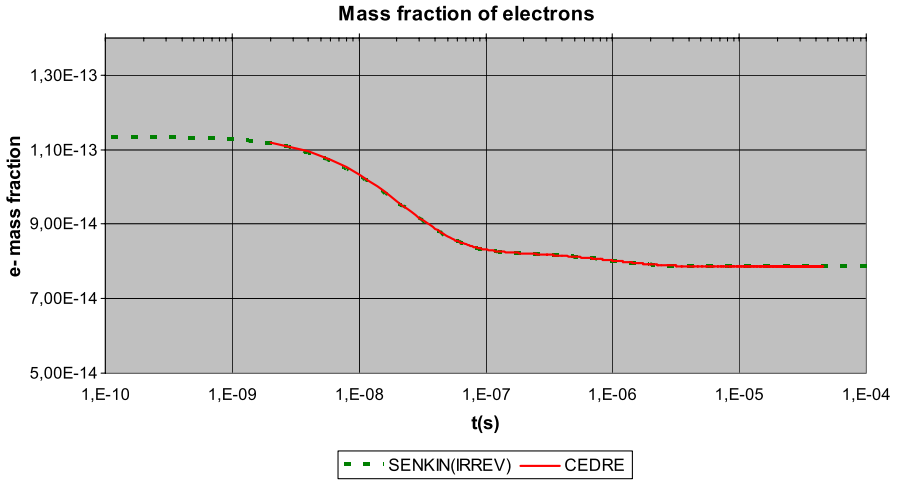

Fig. 4 Time evolution of electron mass fraction using CEDRE and SENKIN.

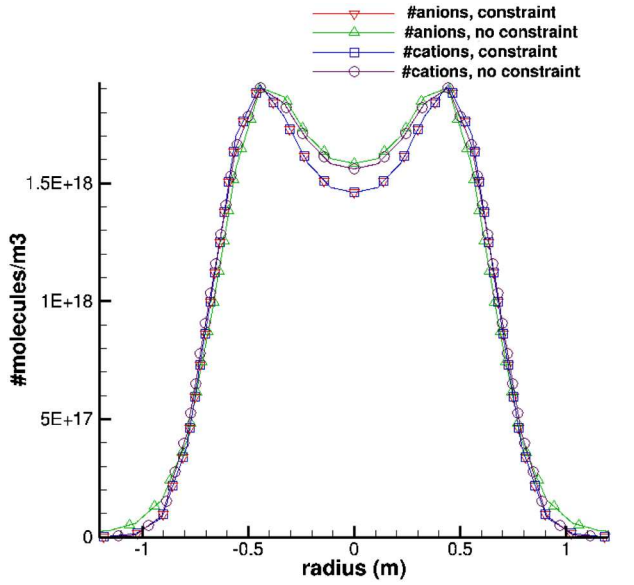

Fig. 5 Concentrations of anions (including electrons) vs cations in a plume cross section, with or without charge constraint.

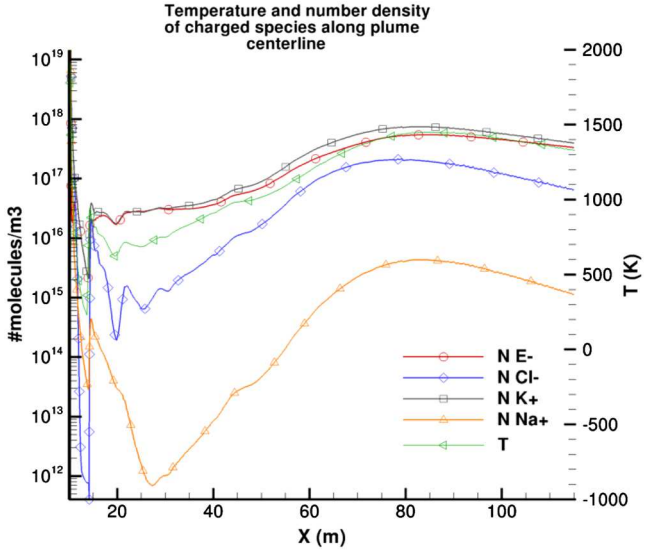

Fig. 6 Temperature (in K, right scale) and charged species concentration (in molecules/m^3, left scale) along the plume centerline.

of the solid propellant from [31] and verified that we obtain correct specific impulse using COPELLIA [36], ONERA's rocket performance code. We have retained the following composition: 19% aluminum, 61% ammonium perchlorate, and 20% HTBP-polyurethane binder.

As in [3], simulations for the validation test case were performed in the absence of alumina particles. We obtain a peak concentration of about 5.5 10^{17} electrons per m^3 at 85 m from the nozzle exit (see Fig. 6), whereas [3] shows a maximum of about 3.10^{17} electron per m^3 at about 42 m. The predicted electron concentration profiles are qualitatively similar to the ones in [3], but our simulations show strong oscillations of charged species concentrations in the Mach disks region close to the nozzle. It should also be noted that [3] only takes into account the influence of the Na+ ion, whereas we take into account K+, Na+, and Cl−. The concentration of Na+ ions in the chamber appears to be about 5.10^{15} molecules per m^3 in [3], whereas it is 10^{16} molecules per m^3 in our study.

Our simulations show a temperature peak of 1400 K at 85 m from the nozzle exit (see Fig. 6), whereas [3] predicts a peak temperature of 1700 K at the same distance (85 m). We observe in all of our simulations that the electron concentration is strongly correlated with the temperature profile. Similar correlation was observed in [7].

VI. Results

A. Electron Density in Rocket Plume

Here, we show computation results for electron density in the plume of a Black Brant rocket at altitude 25.5 and 7.9 km. For the two computations, conditions in the combustion chamber are the same: 45.8 bar pressure and 3290.83 K temperature. Chemical composition of the gas mixture in the combustion chamber is shown in Table 1.

The external flow conditions for the first test case at altitude 25.5 km are as follows: rocket velocity is 1547.7 m/s, atmospheric pressure is 2350 Pa, and atmospheric temperature is 222 K. For the second test case at altitude 7.9 km, rocket velocity is 646.79 m/s, atmospheric pressure is 12,650 Pa, and atmospheric temperature is 216.6 K. In these simulations, the influence of alumina particles has been taken into account.

Figure 7 shows electron concentration at the two altitudes. For both cases, electron concentration is high in the afterburning region, where ionization reactions are activated by high temperatures, and in the turbulent mixing layer between the unburned species and atmospheric O_2. As expected, the mixing layer grows linearly in the first region of the plume and electrons diffuse both upstream and toward the plume core until they reach the centerline.

The electron density profile is highly correlated with the temperature profile. Electron density is high in the afterburning region and in the mixing layer between exhaust gases and fresh air. In particular, maximum electron density is reached near the temperature maximum in the plume. In addition, the plume length and width increases with

Table 1 Chemical composition of fluid mixture in the combustion chamber

Species	Mass fraction, %
H	0.19
O	0.02
OH	0.34
H_2	4.38
H_20	10.04
OH	44.09
CO_2	2.31
HCl	25.05
Cl_2	3.8e − 5
Cl	1.42
N_2	12.16
E−	9.47e − 12
Cl−	3e − 5
K	8.9e − 6
K+	2.9e − 5
Na	1.3e − 5
Na+	2.6e − 6
NaCl	2.9e − 4
KCl	3.5e − 4

increasing altitude and decreasing atmospheric pressure. In fact, with increasing altitude, the nozzle becomes increasingly overexpanded and the plume becomes wider in order for the pressure near the nozzle exit to adapt to the low atmospheric pressure. Moreover, the plume length and the plume temperature decrease with increasing rocket velocity at constant altitude. In fact, with increasing rocket velocity, the difference between plume velocity and exterior velocity decreases. These effects influence the electron density in the plume and ultimately, altitude and velocity strongly influence the radar signature of solid rockets.

B. Influence of Alkali Metal Concentration

Here, we study the influence of alkali metal concentration in the propellant on ionization levels in the plume. We compare electron density in the plume at altitude 25.5 km for two concentrations of alkali metals in the propellant: 100 and 10 ppm. As expected, Fig. 8 shows decreased electron density in the plume with decreased alkali concentrations in the propellant.

C. RCS Calculations

To compute the plume RCS, we have coupled the solver described previously with an electromagnetic code computing the macroscopic Maxwell's equations in harmonic time domain. Diffusion is primarily controlled by the behavior of electrons. Electron number density is denoted by N_e with $N_e = N_A c_{e-}$ and electron temperature by T_e.

The relative dielectric permittivity ε_r is deduced from the expression (see [2,5])

$$\varepsilon_r = 1 - i\frac{\omega_P^2(f_c - j\omega)}{\omega(f_c^2 + \omega^2)} \tag{19}$$

with ω as the radar pulsation, ω_P as the plasma frequency depending on the square root of N_e, $i = \sqrt{-1}$, and f_c as the collision frequency, which reads

$$f_c = \left(\frac{8k_B T_e}{\pi m_e}\right)^{\frac{1}{2}} \sum_s N_s Q_{es} \tag{20}$$

with k_B as the Boltzmann constant, T_e as the electron temperature, m_e as the electron mass, N_s as the number density for species colliding with electrons, and Q_{es} as the electron-species collision cross sections.

We formulate Maxwell's equations for 2-D axisymmetric geometries. Simulation cases consist of perfectly conducting bodies

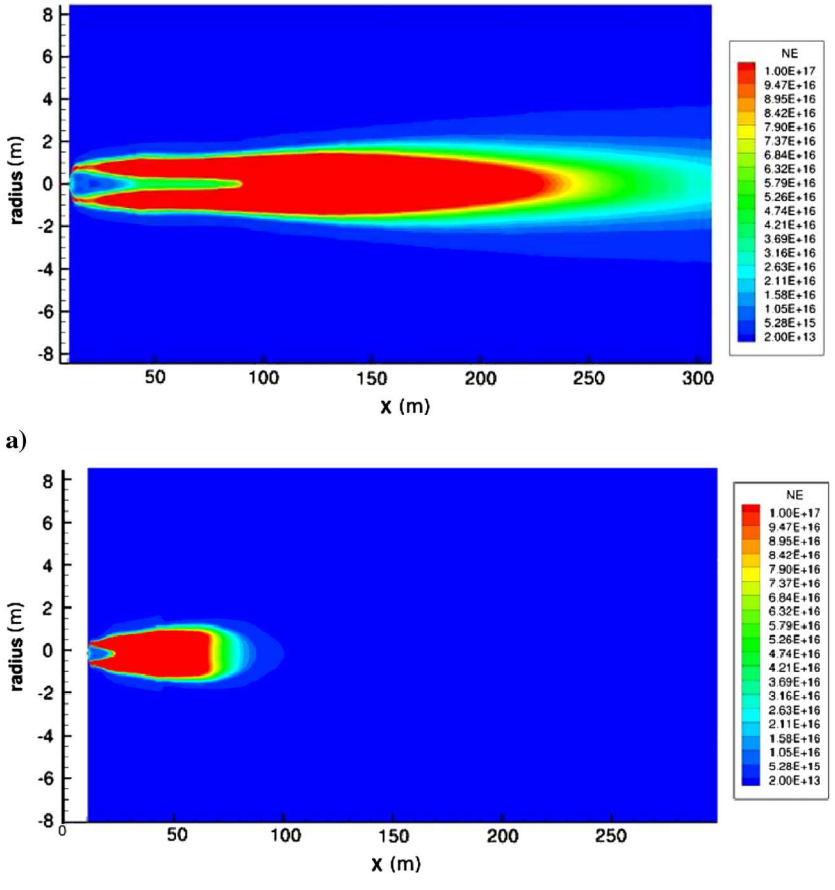

a)

b)

Fig. 7 Electron concentration (e − /m^3) in the plume at altitude a) 25.5 km and b) 7.9 km.

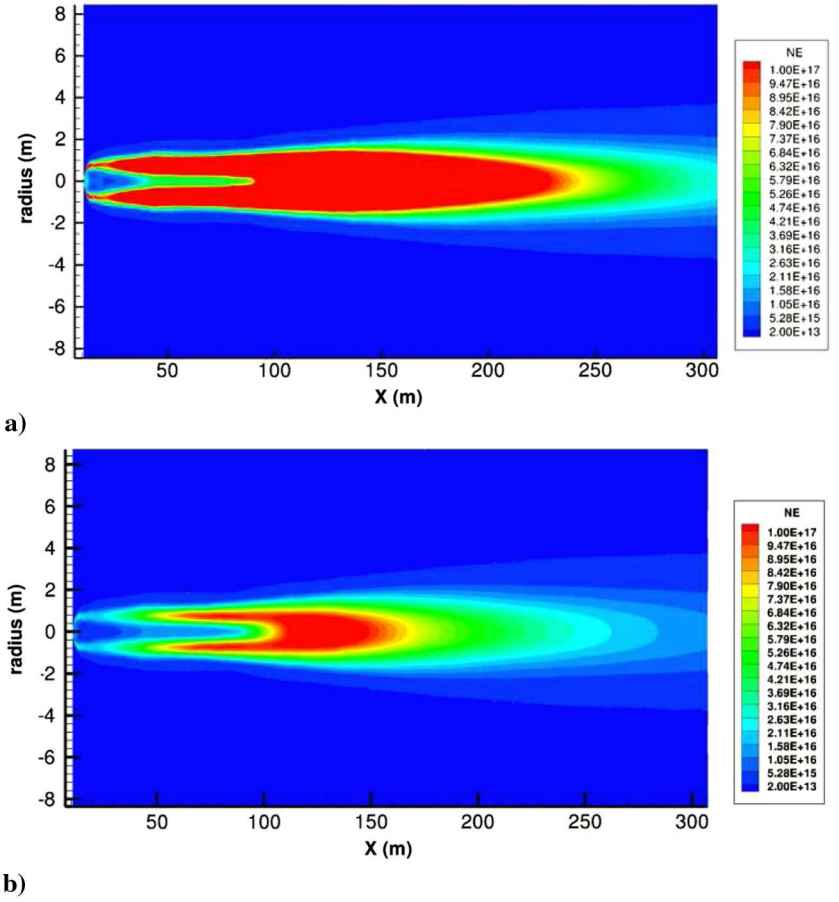

Fig. 8 Influence of alkali metal concentration on ionization level in the plume of a Black Brant rocket.

and of dielectric isotropic materials with or without losses (magnetic and/or electric). The problem is solved using an integral equation formulation on the boundary coupled to a differential equation formulation in the bulk [37,38]. The integral equations are formulated with respect to the unknown scattered electromagnetic fields $\boldsymbol{E}$ and $\boldsymbol{H}$. These integral equations read

$$\begin{cases} -\boldsymbol{E}_{\text{inc}} = -\dfrac{\boldsymbol{E}_{\text{tot}}}{2} + \dfrac{1}{4\pi}\displaystyle\int_{\Gamma}\left(\frac{-i}{k}(\boldsymbol{n}.\mathbf{rot}\boldsymbol{H})\right)\nabla G + (\boldsymbol{n}.\boldsymbol{E}_{\text{tot}})\nabla G - ik(\boldsymbol{n}.\boldsymbol{H}_{\text{tot}})G\,\mathrm{d}\sigma \\ -\boldsymbol{H}_{\text{inc}} = -\dfrac{\boldsymbol{H}_{\text{tot}}}{2} + \dfrac{1}{4\pi}\displaystyle\int_{\Gamma}\left(\frac{i}{k}(\boldsymbol{n}.\mathbf{rot}\boldsymbol{E})\right)\nabla G + (\boldsymbol{n}.\boldsymbol{H}_{\text{tot}})\nabla G + ik(\boldsymbol{n}.\boldsymbol{E}_{\text{tot}})G\,\mathrm{d}\sigma \end{cases} \tag{21}$$

where $\boldsymbol{E}_{\text{inc}}$ and $\boldsymbol{H}_{\text{inc}}$ are the incident electromagnetic fields, $\boldsymbol{E}_{\text{tot}} = \boldsymbol{E} + \boldsymbol{E}_{\text{inc}}$, $\boldsymbol{H}_{\text{tot}} = \boldsymbol{H} + \boldsymbol{H}_{\text{inc}}$, $\boldsymbol{n}$ is the normal to an arbitrary closed Γ surface, k is the wavenumber, and G is the Green's function.

The backscattering RCS at 26 MHz, taking into account collision frequency, is shown in Fig. 9. The Black Brant rocket is at altitude 25.5 km and we assume that the concentration of alkali metals in the propellant is 100 ppm. The two plots correspond to the two polarizations, Theta-Theta (TT) being perpendicular to the direction of the observer and in the plane of the mesh, and Phi-Phi (PP) being perpendicular to the plane of the mesh. Here, 0, 90, and 180 deg correspond respectively to front, side, and rear aspect angle. The high level obtained for all angles but the tail angle and the dissymmetric shape show that the signature differs from the one of a conducting cylinder.

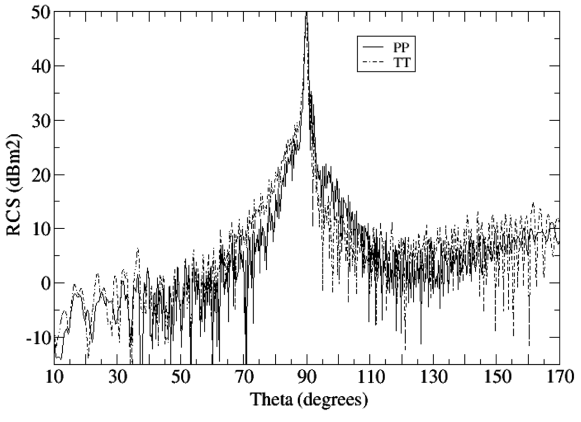

Fig. 9 RCS at 26 MHz for two polarizations: TT and PP.

VII. Conclusions

A model describing the ionized plume of a solid rocket was presented in this paper. The conservation equations describing the ionized flow have been carefully derived and a numerical methodology to resolve these equations was developed. A time implicit scheme has been derived that enforces exact charge neutrality and zero current. Using this approach, good agreement with prior work on the ionized flow in the plume of a Black Brant rocket was obtained. In

addition, the influence of altitude and alkali concentration on the ionization level in a Black Brant rocket plume was studied and the RCS of this plume was computed.

Future work will concentrate on obtaining the turbulent fluctuations of electron and ion densities in order to compute dynamic Doppler signatures. Furthermore, we will conduct in the near future a set of ground experiments and RCS measurements on a small-scale solid rocket motor. These experimental tests will provide additional validations for the numerical and physical models presented in this paper.

Acknowledgments

This research was supported by an ONERA grant (TIS/RGF/PRF/2008/4 — PRECISE). D. Gueyffier thanks Dmitry Davidenko for input on validation test cases, Dominique Scherrer for help with the time implicit scheme, Yves Fabignon for discussions about the ionization model, Isabelle Dubois and Vincent Borie for important data on ionization chemistry and on prior work, Philippe Grenard for rocket performance calculations and grid mesh, and Valerie Haemmerle for rocket trajectory calculation and input data on the Black Brant rocket.

References

[1] Mikatarian, R. R., Kau, C. J., and Pergament, H. S., "Fast Computer Program for Nonequilibrium Rocket Plume Predictions," Aerochem Research Laboratories AD-751-984, 1972.

[2] Nogard, J. D., and Smith, G. S., "A Plasma Model of Missile Exhaust Plume," RADC TR-77-144, Georgia Tech, 1977.

[3] Draper, J. S., and Sperlein, R. F., "Analysis of Radar Returns of a Rocket Plume," *AIAA Journal*, Vol. 18, No. 6, 1980, pp. 712–713. doi:10.2514/3.7679

[4] Lee, R. H. C., Chang, I. S., and Stewart, , "Studies of Plasma Properties in Rocket Plumes," The Aerospace Corporation SD-TR-82-44, 1982.

[5] McMillion, A., "Simple Method for Predicting RF Attenuation Through a Rocket Exhaust Plume," U.S. Army Aviation and Missile Command, Contract No. DAAL03-91-C-0034, 1997.

[6] Bico, J., "Ionisation Dans Les Jets de Propulseurs," ONERA TR RT 12/6129 DEFA/YDEFA 321 B, 1998.

[7] Cousins, J., and Jensen, D., "On the Computation of Ionization Levels in Rocket Exhaust Flames," *Combustion and Flame*, Vol. 52, 1983, pp. 111–125. doi:10.1016/0010-2180(83)90126-8

[8] Nayak, S. K., and Thomas, M. J., "Electrical Characterization of Airborne Vehicle Exhaust Plume," *IEEE Transactions on Dielectrics and Electrical Insulation* Vol. 16, No. 2, 2009, pp. 325–333. doi:10.1109/TDEI.2009.4815160

[9] Giovangigli, V., Graille, B., and Rajagopal, K. R., "Asymptotic Stability of Equilibrium States for Ambipolar Plasmas," *Mathematical Models and Methods in Applied Sciences*, Vol. 14, No. 9, 2004, pp. 1361–1399. doi:10.1142/S0218202504003659

[10] Fromentin-Denoziere, B., Gueyffier, D., and Simon, J., "Numerical Modelling of the Radar Signature of Rocket Exhaust Plumes," *IEEE International Conference on Electromagnetics in Advanced Applications (ICEAA)*, IEEE Xplore Digital Libraries, 2012, pp. 400–403.

[11] Farbar, E., Boyd, I. D., and Martin, A., "Numerical Prediction of Hypersonic Flowfields Including Effects of Electron Translational Nonequilibrium," *Journal of Thermophysics and Heat Transfer*, Vol. 27, No. 4, 2013, pp. 593–606.

[12] Blunck, D. L., Harvazinksi, M. E., Merkle, C. L., and Gore, J. P., "Influence of Turbulent Fluctuations on the Radiation Intensity Emitted from Exhaust Plumes," *Journal of Thermophysics and Heat Transfer*, Vol. 26, No. 4, 2012, pp. 581–589. doi:10.2514/1.T3802

[13] Panesi, M., Magin, T. E., Bourdon, A., Bultel, A., and Chazot, O., "Electronic Excitation of Atoms and Molecules for the FIRE II Flight Experiment," *Journal of Thermophysics and Heat Transfer*, Vol. 25, No. 3, 2011, pp. 361–374. doi:10.2514/1.50033

[14] Gueyffier, D., Fromentin-Denoziere, B., Simon, J., Merlen, A., and Giovangigli, V., "Numerical Simulation of Ionized Rocket Plumes," *44th AIAA Plasmadynamics and Lasers Conference*, AIAA, Reston, VA, June 2013.

[15] Poinsot, T., and Veynante, D., *Theoretical and Numerical Combustion*, 2nd ed., R. T. Edwards Inc., Philadelphia, PA, 2005, pp. 141–142.

[16] Lee, R. H. C., Chang, I., and Steward, G. E., "Studies of Plasma Properties in Rocket Plumes," Air Force Systems Command, Space Division SD-TR-82-44, 1982.

[17] Helmer, M., and Plane, J. M. C., "Experimental and Theoretical Study of the Reaction K + HCl," *Journal of Chemical Physics*, Vol. 91, No. 10, 1993, pp. 561–570.

[18] Chase, M. W., "National Institute of Standards and Technology (U.S.)," NIST-JANAF thermochemical tables, Washington, D.C.: American Chemical Society, 1998.

[19] Ruscic, B., et al., "Active Thermochemical Tables: Thermochemistry for the 21st Century," *Journal of Physics: Conference Series*, Vol. 16, No. 1, 2005, pp. 561–570. doi:10.1088/1742-6596/16/1/078

[20] Chevalier, P., Courbet, B., Dutoya, D., Klotz, P., Ruiz, E., Troyes, J., and Villedieu, P., "CEDRE: Development and Validation of a Multiphysics Computational Software," *1st European Conference for Aerospace Sciences (EUCASS)*, Paper 2.04.03, Moscow, Russia, 2005.

[21] Refloch, A., Courbet, B., Murrone, A., Villedieu, P., Laurent, C., Gilbank, P., Troyes, J., Tesse, L., Chaineray, G., Dargaud, J. B., Quemerais, E., and Vuillot, F., "The CEDRE Software," *Aerospace Lab Journal*, Vol. 2, No. 2, 2011, pp. 1–10.

[22] Troyes, J., Dubois, I., Borie, V., and Boischot, A., "Multi-Phase Reactive Numerical Simulations of a Model Solid Rocket Motor Exhaust Jet," *42nd AIAA/ASME/SAE/ASEE Joint Propulsion Conference and Exhibit*, AIAA Paper 2006-4414, July 2006.

[23] Troyes, J., and Vuillot, F., "Numerical Simulations of Model Solid Rocket Motor Ignition Overpressure Waves," *44th AIAA/ASME/SAE/ASEE Joint Propulsion Conference & Exhibit*, AIAA Paper 2008-5133, 2008.

[24] Toro, E. F., Spruce, M., and Speares, W., "Restoration of the Contact Surface in the HLL-Riemann Solver," *Shock Waves*, Vol. 4, No. 1, 1994, pp. 25–34. doi:10.1007/BF01414629

[25] Doisneau, F., Laurent-Negre, F., Murrone, A., Dupays, J., and Massot, M., "Optimal Eulerian Model for the Simulation of Dynamics and Coalescence of Alumina Particles in Solid Propellant Combustion," *7th International Conference on Multiphase Flow*, University of Florida Digital Collection, 2010.

[26] Gottesdiener, L., Gueyffier, D., Abdelouahab, M., Gatignol, R., and Zaleski, S., "Numerical Simulations of Large Falling Drops," *International Journal for Numerical Methods in Fluids*, Vol. 45, No. 1, 2004, pp. 109–123. doi:10.1002/(ISSN)1097-0363

[27] Gueyffier, D., and Zaleski, S., "Formation de Digitations Lors de L'impact D'une Goutte sur un Film Liquide," *Comptes Rendus de l'Académie des Sciences - Series IIB — Mechanics-Physics-Astronomy*, Vol. 326, No. 12, 1998, pp. 839–844.

[28] Papp, J. L., and Dash, S. M., "Turbulence Model Unification and Assessment for High-Speed Aeropropulsive Flows," AIAA Paper 2001-0880, 2001.

[29] Geuzaine, C., and Remacle, J. F., "Gmsh: A Three-Dimensional Finite Element Mesh Generator with Built-In Pre- and Post-Processing Facilities," *International Journal for Numerical Methods in Engineering*, Vol. 79, No. 11, 2009, pp. 1309–1331. doi:10.1002/nme.v79:11

[30] Chakravarthy, S. R., and Osher, S., "High Resolution Applications of the Osher Upwind Scheme for the Euler Equations," AIAA Paper 83-1943, 1983.

[31] Moyers, R. L., "Ground-Based Signature Measurements of a Black Brant Sounding Rocket," *Proceedings of 3rd NATO/IRIS Joint Symposium*, Quebec City, Vol. 43, Oct. 1998.

[32] Haemmerlé, V., "PRF PRECISE—Fusée sonde Black Brant IX—Données Disponibles pour le cas de calcul 2010–2011," Rapport ONERA, Aug. 2010.

[33] "Black Brant: High Altitude Research Rockets," Canadian Bristol Aerojet, Winnipeg, Canada, rev. 1, June 1962.

[34] Swartz, M., Condor, C. E., Davila, J. M., Haas, J. P., Jordan, S. D., Linard, D. L., Miko, J. J., Nash, I. C., Novello, J., Payne, L. J., Plummet, T. B., Thomas, R. J., White, L. A., Brosius, J. W., and Thompson, W. T., "The SERTS-97 Rocket Experiment to Study Activity on the Sun: Flight 36.167-GS on 1997 Nov. 18," NASA TP-1999-208640, Feb. 1999.

[35] Tough, L. H., "Motor Development for the Black Brant VB," AIAA Paper 1967-1329, 1967.

[36] Bourasseau, B., Code COPPELIA: Version 3.0. Calcul de la Composition de Produits de Combustion Contenant de Nombreuses Phases Condensées, Rapport ONERA RT 40/4386 DEFA/N.

[37] Levadoux, D., Millot, F., and Pernet, S., "New Trends in the Preconditioning of Integral Equations of Electromagnetism," *Scientific Computing in Electrical Engineering*, Springer–Verlag, Berlin, Heidelberg, 2010, pp. 383–394.

[38] Greengard, L., Gueyffier, D., Martinsson, P. G., and Rokhlin, V., "Fast Direct Solvers for Integral Equations in Complex Three-Dimensional Domains," *Acta Numerica*, Vol. 18, No. 1, 2009, pp 243–275.